【Memoirs of Construction Engineering Research Institute Vol.54(papers) Nov.2012】

LARGE-EDDY SIMULATION METHOD FOR FLOWS IN RIVERS AND COASTS CONSTRUCTED ON A CARTESIAN GRID SYSTEM

Akihiko Nakayama

ABSTRACT

A Large Eddy Simulation (LES) method that is applicable to calculation of various flows with a free surface as the upper boundary and solid surface on the bottom is described. The grid system used is a fixed rectangular mesh but the boundary geometry can be of general shape and the boundary surfaces may be hydro-dynamically smooth or rough or with obstacles of various shapes and complexity like those that are seen in natural rivers and in coastal regions, but not with movement of loose bed materials. It is a culmination of model development, trial testing, basic validation and applications to several specific applications made by the faculty and students of Civil Engineering Department of Kobe University over several years and the developed software code is dubbed KULES – river and KULES – coast. This report summarizes the basic equations for the motion and necessary models together with an account of numerical methods used. It also shows some basic validation results and sample application results.

1. INTRODUCTION

Numerical simulation methods of real-life turbulent flows are said to have reached to a stage where many practical flows of engineering and environmental applications can be calculated by readily accessible computers with satisfactory results for many purposes. And as the computer power, the cost and the accessibility improve at the present fast rate, many methods are being applied to variety of flows by many groups of research engineers and scientists accumulating a large amount of experiences and learned lessons. They indicate (for example Leschziner[1] and Launder and Sandham[2]), that methods that simulate the turbulent motion that gives rise to effective stresses and diffusivities in averaged flows, or at least part of it, rather than modeling statistical quantities or integrated quantities, produce more accurate, more detailed and reliable results. As to its costs, which have been blamed as the main reason for opting for other methods, they continue to drop at a fast rate, often faster than the rate of development of alternative theory or improvement of methods. Among various methods of simulation, those that simulate the most important part of the turbulent motion, the large scale motion, and by modeling small scale effects, requires minimal physical and mathematical modeling (e.g. Sagaut [3]). Those that depend on models on quantities that change from one situation to other will continue to suffer from shortcoming that there are no universal laws that apply to all large-scale turbulent motions. Therefore, a natural trend of turbulent flow calculation is to apply the concept of Large Eddy Simulation (LES) of one kind or other (e.g. Grinstein et al.[4]).

Recently, commercial or free open source CFD software packages are becoming popular even in academic communities. Those well-managed or well-exercised packages are not yet customized to be exploited as a LES simulator. Methods suitable for LES are not always the same as more traditional ones. The results are in general grid-dependent and numerical methods and interpretation of results are different as well. Yet theoretically, they give better results as the grid resolution is increased. The limitation will be when there are large differences between the scales of turbulence and the scales imposed by external conditions. We have tried to construct a LES simulation methodology that applies to a group of flows encountered by civil engineers working on problems in natural streams or constructed channels and those in coastal regions, which are characterized by the existence of free surface. We have examined several different approaches, tested them and examined the appropriateness of the results mainly for engineering purposes, and have reached to some standard that can be an alternative to widely circulated packages.

The development of turbulent-flow simulation methods requires a sound basic methodology, unified technique of implementation, and painstaking efforts of removing any small bugs. It requires a consistency of a single developer but needs checking by multiple users. What is described here is one of several LES methods developed and implemented by a group and tested by its members in the civil engineering department of Kobe University over several years and is the one approaching a mature state. It is the one constructed on rectangular mesh in Cartesian

coordinates but made to adapt to various flow situations in river and coastal engineering applications.

While there are many disadvantages known to using fixed rectangular grids to represent flows in natural and complex domains compared with unstructured grid or boundary following mesh systems or even mesh-free methods, many advantages in the formulation and interpretation of the simulated results offered by the fixed grid on Cartesian coordinates are hard to dispose of. The river floods breeching levies and waves running up coasts, for example, are far easier to be represented on fixed grids than on boundary-fitted grids which need redefinition as the water front advances or retreats. Furthermore, efficient methods of formulating boundary conditions on complicated connected and unconnected flow regions that may be moving, are being proposed (e.g. Mittal & Iaccarrino[5]). One inefficiency of using fixed rectangular grid is when the flow domain occupies very small portion of enclosing rectangular region like a narrow and long meandering river reach. This inefficiency which was quite severe when the limitation on the memory space was small, is now not so serious with abundant memory space available on even many small computer systems.

By discretizing on a rectangular mesh, some of the development may be done directly in the finite difference sense without worrying much about the partial differential equations and can be presented clearer in a simpler framework. The formulation of the boundary conditions, for example, is far easier if we restrict to rectangular mesh. The purpose of the present write-up is partially to summarize the methods and document the loosely assembled software dubbed KULES-river and KULES-coast that specialize in simulating free-surface flow on a fixed rectangular mesh basis.

2. LES METHOD IMPLEMENTED IN CATESIAN COODINATES

2.1 Basic governing equations

In an application to flows in natural streams and those in coastal areas, we observe following points. First, the flow regions are very irregular in shape and change in time. Second, the scales of the flow, both spatial and timewise are very large and the spacings of grid points and the time step that can be accommodated by a readily available computer system are nowhere enough to resolve dissipation scales. Yet with a reasonable number of grid points like a few million points, which roughly divide the total flow region into cubes of orders-of-magnitude smaller in length, most of the large-scale flow and a good fraction of the turbulent fluctuations can be resolved from which not only the mean flow but turbulent stresses can be evaluated. That means that the filtered flow with this scale does represent the overall characteristics of the flow being simulated very well.

The filtered equations of motion and the continuity equation for the spatially-filtered velocity components (u,v,w) and the filtered pressure p in rectangular coordinates (x,y,z) with z taken positive vertically upward are

$$\begin{aligned}
&\frac{\partial u}{\partial t}+\frac{\partial u^2}{\partial x}+\frac{\partial uv}{\partial y}+\frac{\partial uw}{\partial z}=-\frac{1}{\rho}\frac{\partial p}{\partial x}+\frac{\partial}{\partial x}\left(\nu\frac{\partial u}{\partial x}+\tau_{xx}\right)+\frac{\partial}{\partial y}\left(\nu\frac{\partial u}{\partial y}+\tau_{yx}\right)+\frac{\partial}{\partial z}\left(\nu\frac{\partial u}{\partial z}+\tau_{zx}\right)\\
&\frac{\partial v}{\partial t}+\frac{\partial uv}{\partial x}+\frac{\partial v^2}{\partial y}+\frac{\partial vw}{\partial z}=-\frac{1}{\rho}\frac{\partial p}{\partial y}+\frac{\partial}{\partial x}\left(\nu\frac{\partial v}{\partial x}+\tau_{xy}\right)+\frac{\partial}{\partial y}\left(\nu\frac{\partial v}{\partial y}+\tau_{yy}\right)+\frac{\partial}{\partial z}\left(\nu\frac{\partial v}{\partial z}+\tau_{zy}\right)\\
&\frac{\partial w}{\partial t}+\frac{\partial uw}{\partial x}+\frac{\partial vw}{\partial y}+\frac{\partial w^2}{\partial z}=-\frac{1}{\rho}\frac{\partial p}{\partial z}-g+\frac{\partial}{\partial x}\left(\nu\frac{\partial w}{\partial x}+\tau_{xz}\right)+\frac{\partial}{\partial y}\left(\nu\frac{\partial w}{\partial y}+\tau_{yz}\right)+\frac{\partial}{\partial z}\left(\nu\frac{\partial w}{\partial z}+\tau_{zz}\right)
\end{aligned} \tag{1}$$

and

$$\frac{\partial u}{\partial x}+\frac{\partial v}{\partial y}+\frac{\partial w}{\partial z}=0\ , \tag{2}$$

where t is time, ρ and ν are the density and the kinematic viscosity of water, g is the gravitational acceleration, and τ_{xx} etc. are the effective stress components representing the effects of the unresolved scales of motion.

Since the movement of the water surface is an important part of the flow feature, we solve the spatially-averaged kinematic equation for the elevation h of the filtered water surface along with the velocity field. If we limit to cases where h is a single-valued function of the horizontal position (x,y), it is

$$\frac{\partial h}{\partial t}+\frac{\partial u_s h}{\partial x}+\frac{\partial v_s h}{\partial y}=w_s+\frac{\partial}{\partial x}\tau_{hx}+\frac{\partial}{\partial y}\tau_{hy} \tag{3}$$

where u_s ,v_s, w_s are the (filtered) velocity components at the water surface, and τ_{hx} and τ_{hy} are the sub-grid scale free surface fluctuation terms that may not be known well but are discussed for example by Shen & Yue[6].

For the cases with appreciable, but not too large, density variations, we use the Boussinesq approximation and replace the gravity term in the right hand side of equations (1) by

$$-\left(1+\frac{\Delta\rho}{\rho_0}\right)g\,. \tag{4}$$

where ρ_0 is the reference density which also replaces ρ in the rest of the equations and $\Delta\rho$ is the deviation from it.

Depending on how the density changes, additional equations for the parameters that determine the density changes are introduced. In the case where the water density is determined by the (small) concentration of mixed fluid with different density, we solve the diffusion equations for the concentration c of the mixed fluid

$$\frac{\partial c}{\partial t}+\frac{\partial uc}{\partial x}+\frac{\partial vc}{\partial y}+\frac{\partial wc}{\partial z}=\frac{\partial}{\partial x}\left(D\frac{\partial c}{\partial x}+\gamma_x\right)+\frac{\partial}{\partial y}\left(D\frac{\partial c}{\partial y}+\gamma_y\right)+\frac{\partial}{\partial z}\left(D\frac{\partial c}{\partial z}+\gamma_z\right)\,, \tag{5}$$

where D is the coefficient of molecular diffusion and γ_x, γ_y, γ_z are the sub-grid transports in x, y and z directions.

2.2 Subgrid model

While a wide range of models for the sub-grid effects have been proposed in the last decade or so (e.g. Sagaut[3]), but after trying a few different variations, we feel a model that is mathematically simple, numerically efficient and less complex in implementation is best for simulating large-scale flows in complex domains than those elaborate ones with extra computational loads. We use the eddy viscosity model with the effective kinematic viscosity ν_{sgs}

$$\begin{aligned}
&\tau_{xx}=2\nu_{sgs}\frac{\partial u}{\partial x}\,,\quad \tau_{xy}=\nu_{sgs}\left(\frac{\partial u}{\partial y}+\frac{\partial v}{\partial x}\right),\quad \tau_{xz}=\nu_{sgs}\left(\frac{\partial u}{\partial z}+\frac{\partial w}{\partial x}\right)\\
&\tau_{yx}=\nu_{sgs}\left(\frac{\partial v}{\partial x}+\frac{\partial u}{\partial y}\right),\quad \tau_{yy}=2\nu_{sgs}\frac{\partial v}{\partial y}\,,\quad \tau_{yz}=\nu_{sgs}\left(\frac{\partial v}{\partial z}+\frac{\partial w}{\partial y}\right)\,,\\
&\tau_{zx}=\nu_{sgs}\left(\frac{\partial w}{\partial x}+\frac{\partial u}{\partial z}\right),\quad \tau_{zy}=\nu_{sgs}\left(\frac{\partial w}{\partial y}+\frac{\partial v}{\partial z}\right),\quad \tau_{zz}=2\nu_{sgs}\frac{\partial w}{\partial z}
\end{aligned} \tag{6}$$

ν_{sgs} is evaluated by the standard Smagorinsky model[7]

$$\nu_{sgs}=C_S\Delta^2\left[4\left(\frac{\partial u}{\partial x}\right)^2+4\left(\frac{\partial v}{\partial y}\right)^2+4\left(\frac{\partial w}{\partial z}\right)^2+2\left(\frac{\partial u}{\partial y}+\frac{\partial v}{\partial x}\right)^2+2\left(\frac{\partial u}{\partial z}+\frac{\partial w}{\partial x}\right)^2+2\left(\frac{\partial v}{\partial z}+\frac{\partial w}{\partial y}\right)^2\right]^{1/2} \tag{7}$$

where Δ is the geometric average of the grid spacings and C_s is the Smagorinsky constant for which we typically take a value of 0.13. The numerical grid we will use is not assumed to resolve the flow near solid surfaces accurately. It is the main feature of flows of civil engineering applications that so-called near-wall flow cannot and will not be able to be resolved by any realistic computer systems that may become available in near future. How the flow in this wall region is treated is as important as how the main equations of motion (1) are solved and how the sub-grid scale effects are modeled. So we describe how the near-wall flow is treated here together with the sub-grid model.

The role of the near-wall flow is how it generates the turbulence that gives rise to resistances. It is known for sometime (e.g. Robinson[8]) that the bursting eddies in this region are responsible for large resistance compared with, say non-turbulent laminar flows. So we use a model that relates the near-wall flow velocity to the wall shear stress on the local and instantaneous basis. Instead of using classical ones proposed by Schumann[9] and improved by few others, which we found, do not fit the instantaneous flow data well (Nakayama et al.[10]) we use the following empirical relation. We found it works well[11], at least as well as other near-wall treatment (Piomelli and Balaras[12] and Leveque et al.[13]) and such as reducing the sub-grid eddy viscosity or using dynamically determined values of eddy viscosity coefficient.

If (u_1,v_1,w_1) are the velocity components calculated at points closest to a solid wall, the Cartesian shear stress components on the wall are written in terms of the velocity as

$$\tau_{xy} = C_d \rho V_1 v_1 , \quad \tau_{xz} = C_d \rho V_1 w_1$$

$$\tau_{yx} = C_d \rho V_1 u_1 , \quad \tau_{yz} = C_d \rho V_1 w_1 \tag{8}$$

$$\tau_{zx} = C_d \rho V_1 u_1 , \quad \tau_{zy} = C_d \rho V_1 v_1$$

where $V_1 = \sqrt{u_1^2 + v_1^2 + w_1^2}$, and C_d is a model coefficient and is evaluated by a friction law for instantaneous flow. It is noted that the above form for the stress does not satisfy the symmetry condition or the Gallilian invariance that are usually required for stresses within flow. It is very specific to be applied to flow close to a solid wall. For now, since we do not know the friction law for fluctuating flow, we use the equations that have been used to relate the mean velocity and the mean wall stress.

$$C_d = \left[A \ln \frac{z_1 u_\tau}{\nu} + B \right]^{-2} , \quad \frac{k u_\tau}{\nu} \le 100 \text{ , and } \frac{z_1 u_\tau}{\nu} > 10 , \tag{9}$$

$$C_d = \left[\frac{z_1 u_\tau}{\nu} \right]^{-2} , \quad \frac{k u_\tau}{\nu} \le 100 \text{ , and } \frac{z_1 u_\tau}{\nu} \le 10 , \tag{10}$$

$$C_d = \left[A \ln \frac{z_1}{k} + C \right]^{-2} , \quad \frac{k u_\tau}{\nu} > 100 \tag{11}$$

where A(=2.5), B(=5.2) ,C(=8.5) are constant. u_τ is the friction velocity defined by the total wall stress τ_w of which components are given by Eq.(8), k is the roughness height and z_1 is the distance to the solid surface. It is noted that Eq.(8) and Eqs.(9)-(11) have to be solved iteratively like 'wall function' method used in two-equation turbulence models (Launder & Sandham[2]).

When the roughness height k is larger than the grid height, and the roughness elements can be resolved by the grid, the effects can be more directly reflected in the boundary geometry. When the exact shape is very complex but the envelope of the distribution may be simple enough to be resolved like trees and vegetation, the effects are modeled by introducing in-flow drag. In such a case we add to the right hand side of Eqs.(1) the body force of the following form

$$f_v = -C_v \Lambda V u , \quad g_v = -C_v \Lambda V v, \quad h_v = -C_v \Lambda V w \tag{12}$$

where C_v is the average drag coefficient, Λ is the average density of surface area that receive the drag force and V is the magnitude of the velocity at a point in the roughness influence area.

As to the sub-grid scale terms τ_{hx} and τ_{hx} in the equation for the free-surface elevation, we use a gradient model[12]

$$\tau_{hx} = -\gamma_{sgs} \frac{\partial h}{\partial x} , \quad \tau_{hy} = -\gamma_{sgs} \frac{\partial h}{\partial y} , \quad \gamma_{sgs} = \gamma \nu_{sgs} \tag{13}$$

where γ_{sgs} is a model coefficient which is taken to be proportional to ν_{sgs} (e.g. Hodges and Street[14]).

2.3 Boundary conditions

Since how the flow near solid boundary is treated has been explained as part of the sub-grid model of unresolved motion, here we describe how the other boundaries are treated.

The free surface is treated as the freely moving boundary and the motion of air above it is ignored. This means that the pressure and the normal viscous stress on the free surface are constant and the shear stress components on the free surface vanish. Since we use the eddy-viscosity model for the sub-grid stresses, zero shear deformation condition assures that both the viscous and the sub-grid shear stresses vanish. The exact application of these conditions is a little more complicated. When such an air-water interaction like wind waves is important we set the shear stress boundary condition. It will be explained in the next section on the numerical method how these conditions are implemented in terms of the Cartesian components on a rectangular mesh.

The surface tension effects and/or the effects of the sub-grid fluctuation of the free surface as indicated in Eq.(3) is important, we apply the condition

$$p + \sigma K = 0 \tag{14}$$

where σ is the coefficient of surface tension and K is the radius of curvature of the free surface positive for convex fluid surface.

For boundaries with clear inflow and outflow sections like that in of river reach, it is assumed that the flow is sub-critical at the upstream inflow and at the downstream outflow sections or take the calculation region to meet this criterion. In the inflow section, the mean-flow velocity component perpendicular to the section is prescribed. If a detailed distribution is not known as the case of river flows, and only the total flow discharge is known, the standard logarithmic profile for fully-developed two-dimensional open-channel flow is assumed at each vertical section across the width of the flow with constant friction velocity. This implies that the velocity takes the maximum value at the free surface and these maximum values are larger at deeper sections.

For reproduction of turbulent fluctuations in the simulated flow, we need to include fluctuating velocity components in the boundary conditions. Turbulent fluctuations appear only after long time and long distances of travel compared with the smallest resolved scales. Therefore we take the fluctuating component some distance downstream of the inflow section and superimpose on the prescribed mean-velocity at the corresponding position in terms of the distance from the bed and from the center of the outflow section. The velocity components parallel to the inflow section cannot be imposed on the staggered-variable scheme but add all fluctuation components on the first calculation points from the inflow section. The latter assumption on the fluctuating component is somewhat rough but is better than imposing purely random fluctuation or even no fluctuation.

For fully-developed flows that are often considered as idealized benchmark validation cases, the periodic boundary condition where the quantities at the inflow and outflow sections are set exactly equal. For the free surface elevation, either the same periodic condition is applied when the coordinates are inclined from the direction of the gravitational acceleration by specifying the 'bed slope', or constant difference is set between the corresponding upstream and downstream sections when there is no gravitational acceleration in the streamwise direction.

For flood flow calculation in which the inflow flow rate takes a prescribed discharge hydrograph, say $Q(t)$ we modify the velocity so that the discharge approaches to the desired value with a relaxation time T_i by solving the equation

$$\frac{\partial u}{\partial t} = \frac{u}{T_i} \frac{Q_i(t) - \int_{S_i} u_n dS}{Q_i(t)} \tag{15}$$

where Q_i(t) is the given discharge at time t, S_i is the area of the inflow section and T_i is the time constant, which we typically set to 50 times computational time step. It is noted that when the time constant T_i is zero

$$\int_{S_i} u_n dS = Q_i(t) \tag{16}$$

at all times. Since the velocity at the plane next to the inflow section is computed by the equations of motion that specifies the time change, condition (16) is known to be too stiff[15].

The free-surface elevation at the inflow section is not prescribed but is computed in the solution process. At the outflow section, a few different forms of the outflow condition have been considered. The first one is the usual free-outflow condition, in which the streamwise gradient of the velocity components are set to zero. In the second method, the water level is set to the given value and the pressure distribution is assumed to be hydrostatic. In the third method, we follow the open-boundary condition often used in calculation of coastal flows with open sea boundary (Blumberg & Kantha[15]). In this method, velocity and the water surface follow the partially-clamped radiation outflow condition. We also use a three-dimensional extension of the more traditional conditions used in one-dimensional flood-flow calculation, in which the water surface is determined from the uniform-flow condition. This is equivalent to the free-outflow condition but is evaluated based on the cross-sectional average velocity. Finally, a condition that is close to the known observed relation between the outflow water depth and the discharge Q_o. For the depth-discharge relation, we typically use the power relation

$$H = C_Q Q_o^r + H_o \tag{17}$$

where H is the mean water surface elevation at the deepest point in the outflow section and is assumed constant across

the section, Q_o is the total flow rate through the outflow section, C_Q, r and H_o are constants taken to fit the existing data. After trying these conditions, the results reported in the next sections are obtained by the power law H-Q relation fitting the observed data.

We allow that the wetting edge either advances or retreats as the flow goes over dry land. No specific condition is needed here but the calculation of the free surface position should consider the possibility that the zero flow depth next to region of nonzero depth can have finite depth and vice versa. How it is done is explained in the numerical method section below.

3. NUMERICAL METHOD

3.1 Difference scheme on rectangular mesh

For various reasons explained above and described below, we formulate our numerical method based on the finite difference method for the Cartesian components of the velocity vector at staggered variable definition positions on a rectangular mesh. In this scheme, the pressure is defined and calculated at the center of a cell while velocity components are computed at the centers of cell surfaces normal to the direction of the velocity components. The conservation of mass is formulated with respect to this cell but the conservation of momentum is formulated with respect to different cubes centered around the point of definition of respective velocity components. Figure 1 shows how the positions where variables are defined on the rectangular grid system. Here $h(x,y)$ is the height of the free surface and z_b (x,y) is the elevation of the bottom solid surface, and the flow is in the region bounded by these two surfaces. $h(x,y)$ and z_b(x,y) are defined, similar to the variables defined at the staggered positions, at the center of cells projected in the vertical direction. So there is no information as to the inclination within a cell, as might be implied in Figure 1.

The basic scheme we use is a fractional step method in which the momentum equations are advanced in an explicit way and the pressure is determined and the velocity is corrected so as to satisfy the continuity equation at the advanced time. If u^* is the time-advanced velocity component in the x-direction from time $t = t^n$ by Δt, it is obtained by the Adams-Bashforth scheme as

$$u^* = u^{n-1} + \Delta t \left(\delta_x p^{n-1} + \frac{3}{2}(f_c^{n-1} + f_v^{n-1}) - \frac{1}{2}(f_c^{n-2} + f_v^{n-2}) \right) \tag{18}$$

where superscript indicates the time step, δ_x indicates the difference form of the derivative in the x direction, f_c is the difference form of the convective terms and f_v is the divergence of the viscous and sub-grid-scale stresses. Similar equations are used to obtain the time-advanced values of other components v^* and w^*. Then the corrected velocity component u^n at time $t=t^{n+1}=t^n+\Delta t$ and the pressure p^n are obtained by the Highly Simplified MAC (HSMAC) iteration scheme (Hirt & Cook[16]). In this method, the corrected u^n and pressure are obtained by iteratively correcting u and p by

$$p^n = p^n + \delta p, \quad \delta p = -\Omega \frac{D^*}{2\Delta t\, W} \tag{19}$$

and

$$u^n = u^n + \Delta t\, \delta p / \Delta x_h \tag{20}$$

where Ω is the acceleration parameter $W=1/\Delta x_h^2+1/\Delta y_h^2+1/\Delta z_h^2$, starting with u^* and p^{n-1} until the divergence D^* over

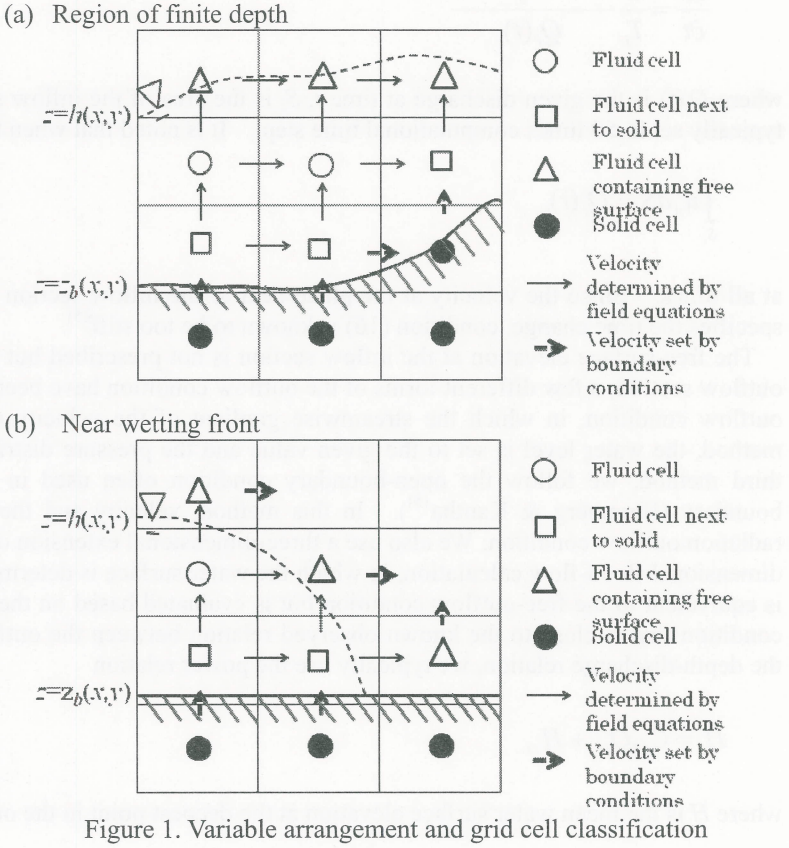

Figure 1. Variable arrangement and grid cell classification

the cell containing the point where p^n is defined, becomes sufficiently small. Here Δx_h etc. are the distances from the center of the cell to the center of the neighboring cell. These procedures are applied to the pressure and velocity associated with the fluid cells designated by circles in Figure 1. For cells containing the free surface designated by triangles, the pressure and the velocity components on the surrounding surfaces are not corrected by Eqs.(19) and (20). The pressure, instead, is prescribed by the free surface pressure condition. The divergence associated with this cell D^* is used to move the position of the free surface by

$$h^n = h^{n-1} - D^* \Delta z \Delta t \tag{21}$$

where Δz is the height of the cell containing the free surface.

This equation amounts to a finite difference form of the equation for h without the sub-grid terms. If the sub-grid terms are added

$$h^n = h^{n-1} - \left[D^* \Delta z - \gamma_{sgs}(\delta_x^2 h + \delta_y^2 h)\right]\Delta t \tag{22}$$

where δ_x^2 and δ_y^2 are the difference forms of the second derivatives in x and y directions.

The actual algorithm turns out very close to the VOF method (Hirt & Nichol[17]) when liquid is assumed to occupy the bottom part of a cell. One difference is that in the present method the free surface position is calculated simultaneously with the pressure and there is no lag in the calculation steps as in most other methods including a level-set method[18]. This way the total volume of fluid can be made to conserve accurately and a stability problem associated with the lag between the steps of velocity calculation and the free surface calculation can be avoided. The validation as to the mass conservation is given in Ref 19).

In the time advancing step, either second-order conservative difference or the third-order upwind difference can be used for differencing the convective terms. The former is preferred but when a variable-spacing grid or coarse grid is used, the latter scheme works better.

With regard to the cells neighboring solid surfaces as indicated by squares in Figure 1, the velocity components normal to the solid surface are set to zero. In the rectangular-mesh formulation, u component, for example, is set to zero on the surface neighboring a solid cell on the right or on the left in the configuration of Figure 1. The tangential velocity components are not specified. The tangential velocity components at their definition points closest to solid surfaces are used to obtain the wall shear stress on the neighboring cell surface that is needed in evaluating terms in f_v, g_v and h_v of the differenced momentum equation for this velocity component.

The cells that contain the wetting front will need a separate treatment. An example of variable arrangement in this case is shown in Figure 1(b). In order to correctly calculate the movement of the wetting front, the horizontal velocity component at the vertical surface (the surface bordering cell indicated by a square and that indicated by a triangle in Figure 1(b)) of the cell containing the wetting front must be computed according to the equation of motion. This means that the pressure next to the front-containing cell must be set so that the horizontal pressure gradient is evaluated. In order to do this, the pressure at the center of the cell outside of the front-containing cell is set by using the boundary condition that the pressure at the front is atmospheric or zero. This amounts to the same treatment as other cells designated as the fluid cell containing free surface.

There is one other complication. If the surface tension and wetting effects of liquid are not considered, the wetting front should move instantly along a smooth horizontal or down slope surfaces. The present scheme allows one cell at one time step. Since the time step is usually taken to satisfy the Courant number requirement and the speed of propagation of surface wave, the speed of propagation is faster than the fluid velocity itself. In most applications, however, the surfaces are geometrically rough. Small roughness elements will retard the movement of the front not by the shear stress but by pressure force on the vertical sides of the roughness elements. In the present method, it is assumed that there are small protrusions of height some fraction of the roughness height which in turn is a fraction of the thickness of the numerical grid. With this assumption, the rate of flooding can be reproduced very well but on a smooth surface it propagates one cell per one time step.

The variable arrangement and the calculation procedure near the other boundaries such as upstream and downstream and open boundaries are done as follows. The boundaries are classified as either those where the velocity or the total discharge or those where the elevation of the free surface is specified. The velocity components normal to the boundary is specified directly at the definition position. Tangential velocity components are not defined on the bounding surfaces, they do not have to be defined or should not be. However pressure and the free surface elevation gradients may be specified at the boundary. This is done by extending cells just outside the boundary and set the values at the center of these extended cells so that the normal gradient becomes the desired value. It is done to specify tidal elevation. Also for uniform flows in a long channel, the surface gradient is set equal to the bed shear. In case of setting the downstream elevation directly or by a stage-discharge relation as described in the previous section, the values at the center of extended cell is set so that the value on the boundary becomes the desired value.

As to the fluctuation components of velocity and pressure, those at the inflow boundaries are either fed back from some distance downstream or by setting an approach section where turbulence is made to develop by applying periodic boundary condition at the inflow and outflow boundaries of the approach section. Those at the outflow section are allowed to translate by using the radiation condition.

4. VALIDATION CALCULATION OF BENCHMARK FLOWS

The present method has been tested in several basic flow configurations. Like validations of most new sub-grid models and numerical methods, we first show the results of calculation of a fully-developed open-channel flow. In the present case we use a case laboratory experiment at large enough Froude number so there is a free surface fluctuation. The fully developed turbulent flow in a flat open channel measured by Nakayama[20] is chosen. Two different grid spacings are used. The first one is a coarse grid of 50x40x30 in the streamwise, lateral and vertical directions, respectively. The near-wall grid spacing is as large as 35 wall units. The second grid is a finer 66x64x112 grid and the near wall is resolved to 3.0 wall units. Calculations are started with a velocity distribution with random fluctuations and in a constant depth channel. The periodic boundary conditions are applied in both streamwise and the lateral directions. The Reynolds and Froude numbers based on the mean depth and the average velocity are 20,000 and 1.20, respectively, which correspond to a case of experiments done by Nakayama [20]. The channel bed slope is adjusted to obtain the required flow rate.

The calculated mean streamwise velocity U is plotted in the wall coordinates in Figure 3(a) and in linear scale in terms of the average cross-sectional velocity U_m in Figure 3(b) together with the experimental results. The friction velocity u^* used in these plots (different from u^* in Eq.(18)) are calculated from the channel bed slope. The velocity in the logarithmic layer is seen to lie above the standard log-law or the experimental data. The fine-grid result is

(a) mean velocity distribution in wall coordinates

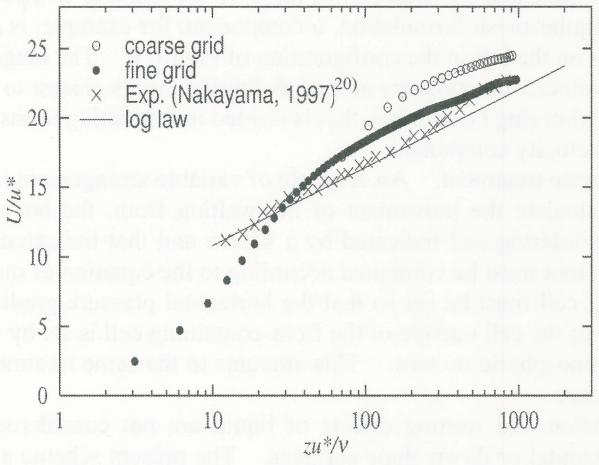

(b) mean velocity distribution in linear scale

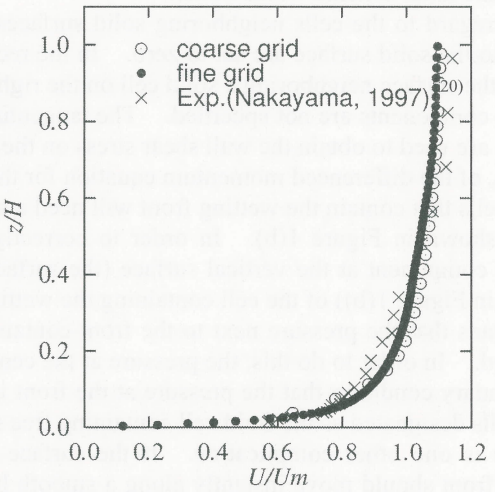

(c) turbulent intensity distributions

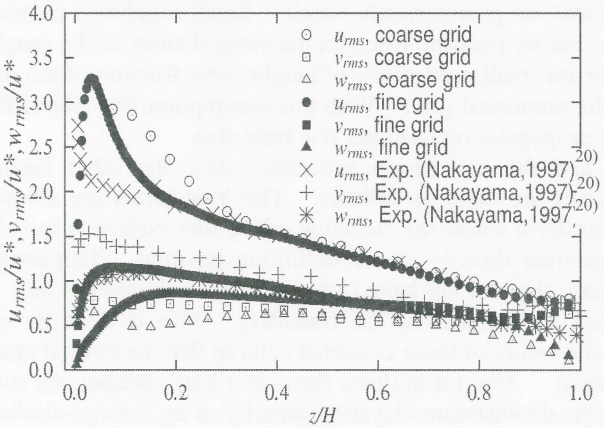

Figure 2. Mean velocity and turbulence intensity distributions in a fully developed open-channel flow for Re=20,000, Fr =1.2.

closer to the experiment and the standard log-law but not by a large margin. The linear plots of the mean velocity of the two runs, however, are not much different. It means that although the wall shear stress is under-predicted by the present method with a grid not sufficiently resolving the near wall region, the overall velocity profile is calculated fairly well.

The calculated turbulent intensities normalized by the friction velocity are shown in Figure 3(c), again compared with the same experiment. The streamwise intensity is seen to be over-predicted with the peak positions farther away from the wall, and the transverse and the spanwise intensities are under-predicted. The results with the finer grid are closer to the experiment. These trends are consistent with the previous calculations of closed-channel flow with Smagorinsky models (e.g. Froehlich & Rodi included in Ref.2)). Near the free surface, there are some differences between the calculation and the experiment.

In the present calculation we have ignored the sub-grid surface fluctuation terms in (6) and the effects of free-surface on the eddy viscosity are not taken into account and these may be the reason for the differences. However, the known characteristics of the non-zero vertical fluctuation and the increased lateral fluctuation near the free surface are reproduced correctly.

As the second validation case, we compute the flow in a straight rectangular channel with side walls. This case will validate the implementation of the side boundaries. Direct Numerical Simulation (DNS) results of a flow in a square channel with vertical side walls and the rigid free-slip surface as the upper boundary have been conducted by Joung & Choi[21] and the results may be compared. By computing this flow we can examine how well secondary flows may be computed that are influenced by the boundary condition on the side walls. We compute the same flow with the present LES method but allowing fluctuation of the free surface. So we set the channel slope instead of imposing the pressure difference between the upstream and downstream sections normally done when the free surface approximated by a rigid lid.

The computational region is similar to Joung & Choi calculation and periodic conditions for all velocity components, the pressure and the depth are applied. The number of grid points is 120 x 100 x 88 and the distance from the wall to the closest calculation point is about 30 wall units. The channel bed slope is set to 1/1000 with periodic conditions between the upstream and downstream ends, which results in the flow such that the Froude number Fr based on the mean velocity is 0.28 and the Reynolds number Re of 110000 about ten times the DNS. The initial velocity distribution and the free surface shape are taken from the results of the first validation case without side walls with the width of the flow same as the average depth. The average depth H obtained after computation is slightly smaller than the width but less than 0.1% and the difference is considered negligible.

Figure 3 shows a sample of instantaneous velocity distributions together with the variation of the free surface elevation. Figure 3(a) is the velocity distribution close to the free surface. Relatively constant velocity and boundary-layer-like disturbances near the walls are seen. The free surface fluctuation is seen smoother than those of the streamwise velocity but more small-scale variations are seen near the side walls. The instantaneous profiles near the bottom (Figure 3(b) show fast and slow flow streaks, typical of wall-shear flows, four or five of them across the width of the flow. These are related to the secondary flow pattern in the time-averaged flow.

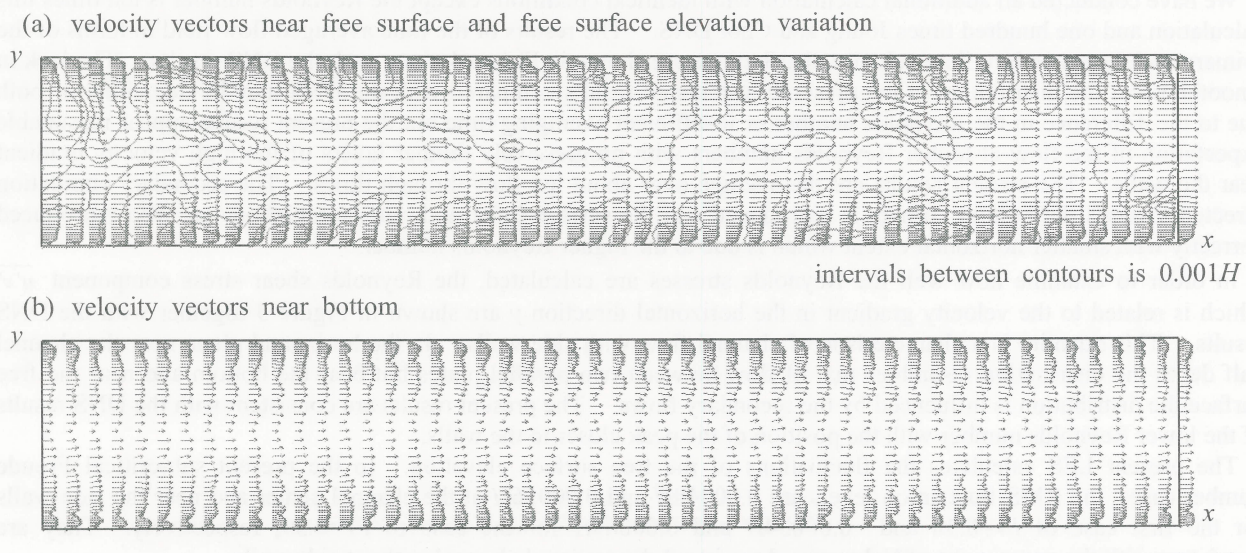

Figure 3. Sample of simulated instantaneous flow.

(a) DNS by Joung & Choi[21], Re=1.0x10^4, Fr=0 (b) present LES Re=1.1x10^5, Fr=0.30 (c) present LES Re=1.1x10^6, Fr=0.39

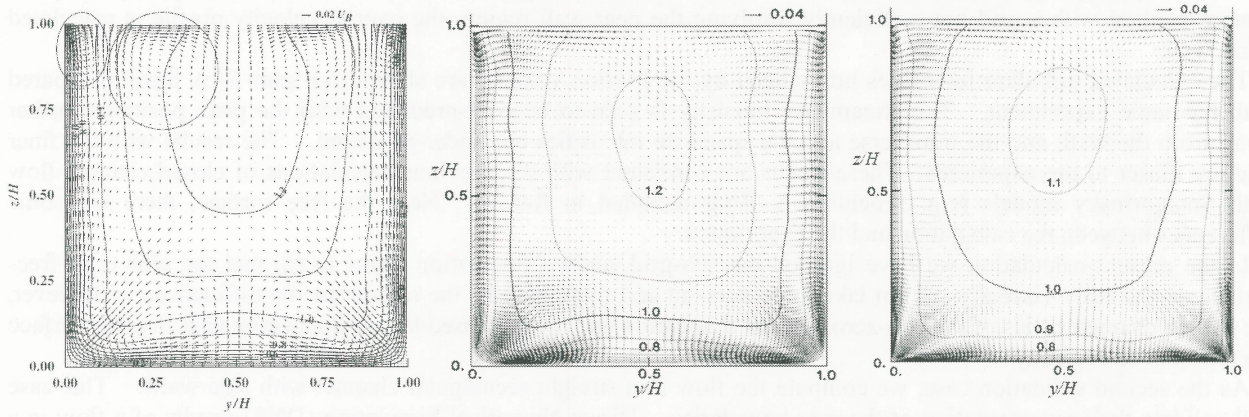

Figure 4. Mean primary and secondary flows, contour values are mean streamwise velocity normalized by the bulk average velocity.

(a) DNS by Joung & Choi[20], Re=1x10^4, Fr=0 (b) present LES Re=1.1x10^5, Fr=0.30 (c) present LES Re=1.1x10^6, Fr=0.39

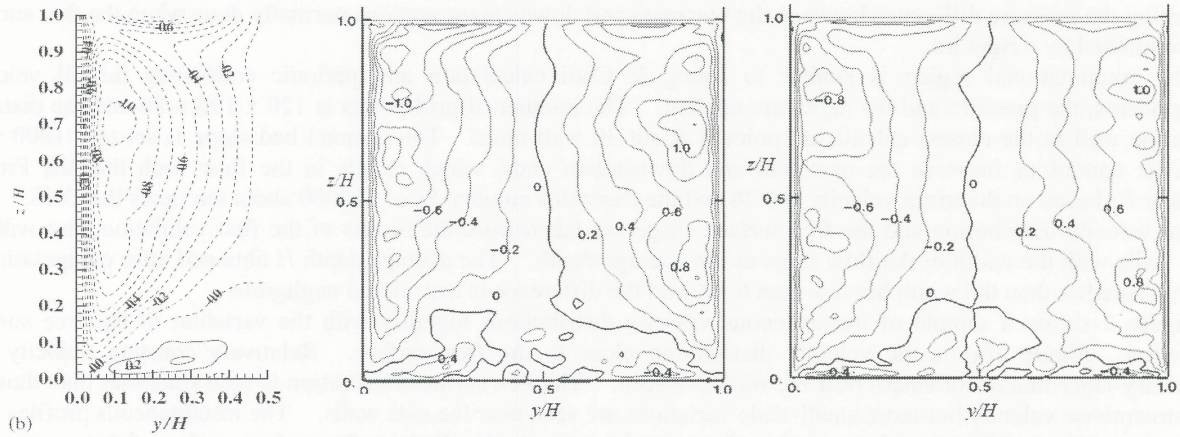

Figure 5. Reynolds shear stress component $\overline{u'v'}$, normalized by the average wall shear stress τ_w.

We have conducted an additional calculation with identical conditions except the Reynolds number is ten times this calculation and one hundred times Joung and Choi DNS. The results of the time averaged flow field in terms of the primary and the secondary flow velocity distributions are shown in Figure 4 along with the DNS results. The lack in smoothness of the distribution in the presently calculated results compared with the DNS may be due either or both due to the difference in the Reynolds number or insufficient averaging time but the present results appear reasonable expectation of the flow at higher Reynolds numbers with progressively thinner layers of the high velocity gradient near the walls. The present results are the average over about ten flow-through times. The secondary circulation directed towards the bottom corners is reproduced and the surface inner and outer circulations are also reproduced correctly with smaller horizontal extent which is due to the higher Reynolds number.

In order to examine how well the Reynolds stresses are calculated, the Reynolds shear stress component $\overline{u'v'}$ which is related to the velocity gradient in the horizontal direction y are shown in Figure 5 together with the DNS results. This quantity is a characteristic of channel flow with side walls. In the horizontal plane near the channel half depth the distribution resembles that of flow between two parallel plates but bear the bottom and near the free surface the distribution is influenced by the secondary flows. The present results are consistent with the DNS results of the lower Reynolds number with the position of the peak closer to the walls.

The present LES calculates the fluctuations of the free surface elevation. In the present sub-critical Froude number cases, the RMS fluctuation levels are 0.00040H and 0.00056H at the channel center and near the side walls for the first case of Fr=0.30 and 0.00034H and 0.00069H for the case of Fr=0.39, respectively. They are consistent with the experiment of Nakayama done in a 2 dimensional channel without side walls.

Next, in order to examine if the movement of the wetting front and larger free surface motion are calculated correctly, the motion of solitary wave running up a slope is then calculated. Comparison is made with an inviscid-flow calculation by Nishimura & Takewaka[22]. Present calculation is done with a prescribed time progress of the flow rate at the section of incident wave starting at the initial water at rest. The viscosity is set so that the Reynolds number based on the initial depth and the maximum flow speed of approximately 10000. No turbulent fluctuations

(a) calculation by Nishimura & Takewaka [22], at t=1.74s (upper) and 2.19s.

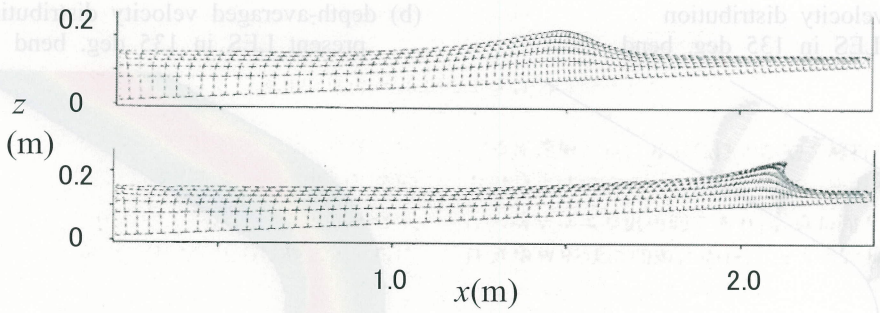

(b) present calculation at t=1.7s and 2.2s

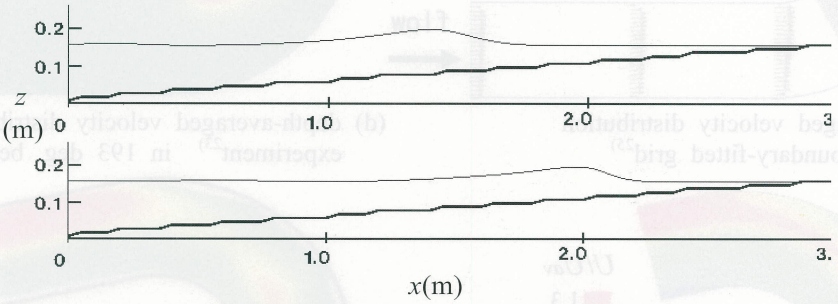

Figure 6 Solitary wave running up a slope, comparison with Lagrangian method.

are introduced either in the initial flow or inflow section and the simulated flow is non-turbulent. The main purpose in this calculation is to examine if the free surface movement is reproduced well and not meant to reproduce fluctuations.

Figure 6(a) shows the results obtained by Nishimura & Takewaka[22] using a Lagrangian coordinate method assuming inviscid flow on perfectly smooth surface. Figure 6(b) shows the results of the present calculation which includes the region where the bed is dry to show the wetting front. In the present calculation, the bed is assumed smooth so that the position of the wetting front is where the pressure gradient balances the gravity. The two calculation results agree very well at t=1.74s when the wave is mild but at t=2.19s when the wave front becomes peaky the free surface of present results is smoothed a little. This is considered to be the difference between the ideal friction-free calculation and with a finite Reynolds number.

One concern that is often raised when a rectangular mesh is used to represent curved boundaries is how sensitive the near wall as well as the overall flow results are to the boundary conditions set at staggered positions not perfectly coinciding with the real boundary. In the present method, the near wall flow is modelled and the zero flux and shear stress condition is used instead of the no-slip condition as explained in the previous section. In order to demonstrate the degree of accuracy of this type of boundary condition used in rectangular grid, we calculated a flow around a channel bend with curved walls. The cross section is a 1.3m wide rectangle and the average depth of flow is 0.15m. The flow in 193 degree circular bend with the radius of the curve of 1.7m of this channel has been investigated by Blanckaert[23] and Zeng et al. [24] and Inokuma et al. [25] both computed the flow using boundary-fitted curved coordinates. Since it involves some modification in the present calculation code to calculate the case of more than 180 degree bend, we modified it to 135 degree bend keeping all other parameters same as the experiment of Blanckaert[23] so comparisons can be made, though not precise, with the experiment and the corresponding calculations using curved coordinates (Figure 7). The grid size is 222x192x70 with equally-spaced mesh in the horizontal directions with the spacing of 0.03m and variable grid spacing in the vertical direction with the minimum grid size of 0.5mm near the bottom. Two channel-width long section downstream of the inflow entrance is used to develop turbulence with the periodic boundary condition as explained in the previous section. In this configuration less than 20 percent of the entire grid points fall within the flow and the rest are not used.

Figure 7 shows the results of the present method in terms of the distributions of the velocity vectors on the free surface and the depth-averaged velocity U normalized by the bulk average velocity U_{av}. The surface velocity is an instantaneous snapshot which appears reasonable without noticeable disturbances. The depth-averaged velocity distribution is qualitatively in agreement with the experiment and the LES using boundary fitting coordinates but the flow appears accelerating more than the experiment or the boundary-fitted LES.

Although not shown here, calculations of flow of collapsing water column and flow impinging on large obstacles and few other flows have been done with satisfactory results (Nakayama et al. [26]).

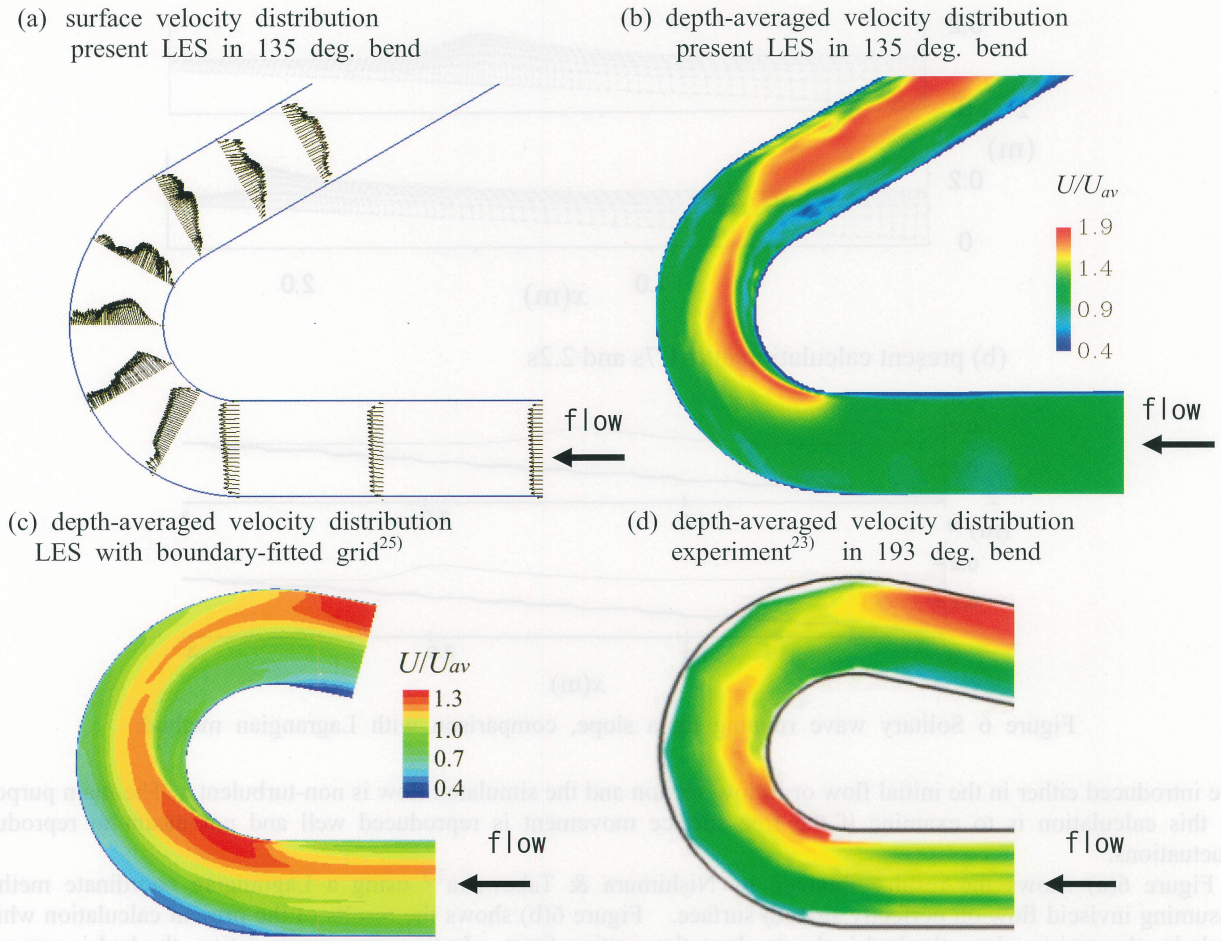

Figure 7. Flow around a circular bend of a channel with rectangular cross section. Comparison of present LES, LES using curved coordinates (Inokuma et al.[25]) and experiment of Blanckaert[23].

5. EXAMPLE SIMULATION OF RIVER FLOW

As an application to flows in a real river we consider the flow at normal time and during a flood in a middle reach of a meandering river Ibogawa River located in western Japan. It meanders in a mountainous region and in dry seasons the gravel bar developed on the inner bank of the bend is exposed but it is washed during floods[23]. There is a small tributary that flows into the main flow just downstream of a bend. Figures 6 show the aerial photographs of this river during a dry season and during a flood. We simulated a reach of about 500m in length around a bend. For the LES calculation, the upstream 100m was extended to let the turbulence develop in the approach section where a periodic recycling boundary condition is applied. The initial condition was chosen to fit a flow rate of 100 m^3/s but the calculation was continued to settle at a steady state. Then we applied a hydrograph at the upstream section and a known depth-discharge relation at the downstream section. When the discharge is about $80m^3/s$ the flow is like that shown in Figure 6(b).

The computational grid we used is 274 x 280 x 73 grid points to resolve 2mx2m in horizontal directions and 0.15m in the vertical direction. About 120 largest boulders were resolved by this grid. Also in the simulation of flood flow that inundates the sand bar on the right bank around the bend where bushes exist, the effects of the bushes are simulated by the resistance model explained in section 2.2.

Sample of results are shown in Figure 6(b) and (d), under conditions that roughly correspond to the photographed flows shown in Figures 6(a) and (c). For these results, a steady state is first obtained for the discharge slightly larger than normal dry season, $100m^3/s$ by computing for about 200 seconds of real time, which is about twice the time flow takes to flow through the calculated reach. Then the discharge is reduced following a typical receding curve. The results shown in Figure 6(b) are obtained when the discharge rate is $80m^3/s$. Though details are not shown, the typical features of the bend with faster flow outside and higher water surface are reproduced.

The results of Figure 6(d) are obtained when the discharge is maintained at 900 m^3/s after increasing is at a rate of $40m^3/s$ every 60second. This is to simulate the flood of Aug 10, 2009 when the photograph of Figure 6(c) was taken when the discharge dropped to about $600m^3/s$ from the peak discharge of $1600m^3/s$. The extent of the area

(a) aerial photo when discharge is about $50m^3/s$

(b) simulation results, instantaneous flow when discharge 80 m^3/s

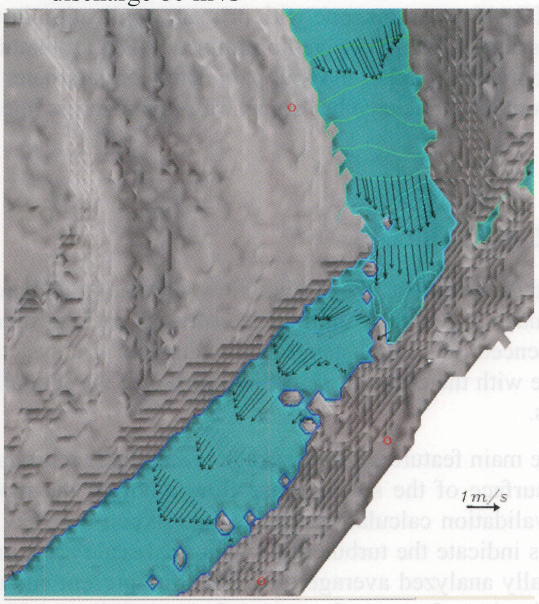

(c) aerial photo during flood of discharge about $600m^3/s$

(d) simulation results, averaged flow when discharge is 900 m^3/s

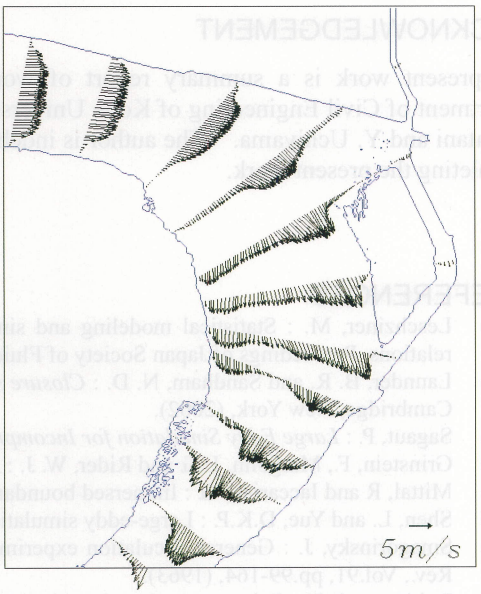

Figure 8 Aerial photographs and corresponding simulation results of flow around a bend of Ibogawa River in western Japan.

submerged under water is indicated by the edge of the inundated region. The water surface elevation was gauged at three locations and the computed elevation was close the observed. At this discharge significant fraction of the discharge flows along the passage behind the gravel bar near the inner bank. It is noted that the flow velocity is still small around the center of the gravel bar. This position corresponds roughly to the points where *A. margaritacea,* community a typical gravel-bar plant in Japan but one suffering heavy damages in recent years , survived the floods of recent years [27]. The simulation of the flow in this river reach has been done for various conditions and will be reported separately.

6. NOTE ON SOFTWARE

What have been explained in the previous section of this report have been put in two separate but very similar FORTRAN programs, one with primary application in mind for hydraulic engineering involving . It still is in serial processing only and not well optimized. But all features described for constant density flow are in a single program with options set either in input parameters or parameter choice at the start of execution. It is therefore very close to a self-contained package but not as well organized as open softwares and far from commercial ones.

7. CONCLUSIONS

The latest turbulent free-surface flow simulation technique of LES has been developed, tested, put to real applications and made a generally applicable software package that is dubbed KULES. It is build on the Cartesian basis and differenced on a fixed staggered rectangular grid system but can adapt to general boundary shapes at a low order but in line with the concept of LES to reproduce the spatially filtered flow field in a smoothed flow region within the grid scales.

The main feature of this package is a realistic reproduction of large-scale turbulent motion and the movement of the free surface of the single-phase flow ignoring the motion of fluid that would exist above the presumed interface. The validation calculations results are shown in a few basic flows and an example simulation case is shown. The results indicate the turbulent flows in real scale are simulated satisfactorily for engineering purposes. In addition to normally analyzed average quantities, the present simulation results contain fluctuations that may be required in the examination of temporal extreme flow conditions. Various physical and thermal effects including the bed sediment and the heat transfer can be readily included as they become necessary in various applications, and the present overall method may be used as an alternative or as an improved CFD method to more widely available packages.

.

ACKNOWLEDGEMENT

The present work is a summary report of work contributed by former students and graduate students of the department of Civil Engineering of Kobe University with suggestions and comments given by Professors I. Fujita, T. Kawatani and Y. Uchiyama. The author is indebted to these students and colleagues and acknowledges their help in completing the present work.

REFERENCES

1) Leschziner, M. : Statistical modeling and simulation of turbulent separated flows: limits, hard lessons and symbiotic relations, Proceedings of Japan Society of Fluid Mechanics Annual Meeting 2007, paper AM0-00-000, (2007).
2) Launder, B. R. and Sandham, N. D. : *Closure strategies for turbulent and transitional flows*, Cambridge University Press, Cambridge, New York, (2002).
3) Sagaut, P. : *Large Eddy Simulation for Incompressible Flows, 3rd ed.*, Springer-Verlag, Berlin Heidelberg, (2006).
4) Grinstein, F., Margolin, L.G. and Rider, W. J. : *Implicit Large Eddy Simulation*, Cambridge University Press, (2007).
5) Mittal, R and Iaccarino, G. : Immersed boundary methods, *Annu. Rev. Fluid Mechanics*, Vol. 37, pp. 239-261, (2005).
6) Shen, L. and Yue, D.K.P. : Large-eddy simulation of free-surface turbulence. *J. Fluid Mech.* Vol. 440, pp.75-116, (2001).
7) Smagorinsky, J. : General circulation experiments with the primitive equations. I. The basic experiment, Mon. Weather Rev., Vol.91, pp.99-164, (1963).
8) Robinson, S. K.: Coherent motions in turbulent boundary layer, *Annu. Rev. Fluid Mech.* Vol. 23, pp.601-639, (1991).
9) Schumann, U., Subgrid scale model for finite difference simulation of turbulent flows in plane channels and annuli, *J. Comput. Phys.* Vol.18, pp.376-404, (1975).
10) Nakayama, A., Noda, H. and Maeda, K.:Similarity of instantaneous and filtered velocity fields in the near wall region of zero-pressure gradient boundary layer, *Fluid Dynamic Research*. Vol. 35, pp.299-321, (2004).
11) Kasai, T. and Nakayama, A. :Study of Model in LES Calculation of Turbulent Flow Over Complex Boundary, *Journal of Hydroscience and Hydraulic Engineering*. Vol.28.No1, pp.117-125, (2010).
12) Piomelli, U. and Balaras, E. : Wall-layer models for large-eddy simulations, *Annu. Rev. Fluid Mech*, Vol. 34, pp.349-374, (2002).
13) Leveque, E, Toschi, F. Shao, L. and Bertoglin, J. P.: Shear improved Smagorinsky model for large eddy simulation of wall-bounded turbulent flows, *J. Fluid Mech.*, Vol. 570, pp.491-502, (2007).
14) Hodges B.R. and Street, L. R.: On simulation of turbulent nonlinear free-surface flows, *J. Comp. Phys.* Vol. 151, pp.425-457, (1999).
15) Blumberg, A. F. and Kantha, I.H. : Open boundary condition for circulation models, *J. Hydraul. Eng.*, Vol.111(2), pp.237-255, (1985).
16) Hirt, C.W., Cook, J.L. : Calculating three-dimensional flow around structure and over rough terrain. *J. Comput. Phys.* 10, 324–340, (1972).

17) Hirt, C.W. and Nichols, B.D.: Volume of fluid (VOF) method for the dynamics of free boundaries, *J. Comput. Phys.* Vol.39, pp.201-225, (1981).
18) Sussman, M. Smereka, E. and Osher, S.:A level set approach for computing solutions to incompressible two-phase flow. *J. Comput. Phys.*, 114, pp.146-159, (1994).
19) Nakayama, A., Matsumura, T. and Hisasue N.:Large-Eddy simulation of turbulent open-channel flow with free-surface fluctuations, Proc. 7th International Conf. on Hydroscience and Engineering, pp.116-117, (2006).
20) Nakayama, T. : Turbulent structures and characteristics of coherent vortices near the free-surface, MS thesis, Dept. Global Environment Engineering, Kyoto Univ., Japan, (1997), (in Japanese).
21) Joung, Y. and Choi, S.-U.: Direct numerical simulation of low Reynolds number flows in an open-channel with side walls, *Int. J. Numer. Meth. Fluids,* Vol.62, pp.854-874., (2012).
22) Nishimura, H. and Takewaka, S.: Numerical analysis of two-dimensional wave motion using Lagrangian description, *proceedings of ASCE* Vol.II-9,191-199, (1988), (in Japanese).
23) Blanckaert, K.:Flow and turbulence in sharp open-channel bends, PhD thesis Nr2545, Ecole Polytechnique Federale Lausanne, Switzerland (ftp://lrhmac15.epfl.ch/Pib/rthesis/Blanckaert/PhD), (2002).
24) Zeng, J, Constantinescu, G. Blanckaert, K. and Weber, L. : Flow and bathymetry in sharp open-channel bends: experiments and predictions, Water Resources Research, Vol.44, W09401, (2008).
25) Inokuma, H., Kuriyama, T. and Nakayama, A.: LES simulation of flow in a curved channel considering motion of the free surface, Abstracts of Third International Symposium on Shallow Flows, pp.253-255, (2012).
26) Nakayama, A., Hisasue, N., Asami, K. and Yokojima, S.: LES simulation of shallow flow with partially submerged objects, Abstracts of Third International Symposium on Shallow Flows, pp.454-456, (2012).
27) Asami, K., Akamatsu, H., Fukui, S., and Tamura, K.,: Morphological characteristics of flood refugia of cobble-bed vegetation, *Journal of Hydro-environment Research*, Vol.6, pp.127-136, (2012)..

AUTHOR

Akihiko Nakayama Staff, Ph.D., Fluid Mechanics, Hydraulics